

Thomas-Fermi Approximation for a Condensate with Higher-order Interactions

M. Thøgersen,¹ N. T. Zinner,² and A. S. Jensen¹

¹*Department of Physics and Astronomy, University of Aarhus, DK-8000 Aarhus, Denmark*

²*Department of Physics, Harvard University, Cambridge, Massachusetts 02138, USA*

(Dated: November 11, 2018)

We consider the ground state of a harmonically trapped Bose-Einstein condensate within the Gross-Pitaevskii theory including the effective-range corrections for a two-body zero-range potential. The resulting non-linear Schrödinger equation is solved analytically in the Thomas-Fermi approximation neglecting the kinetic energy term. We present results for the chemical potential and the condensate profiles, discuss boundary conditions, and compare to the usual Thomas-Fermi approach. We discuss several ways to increase the influence of effective-range corrections in experiment with magnetically tunable interactions. The level of tuning required could be inside experimental reach in the near future.

PACS numbers: 03.75.Hh, 03.75.Lm, 67.85.Bc

I. INTRODUCTION

The Gross-Pitaevskii (GP) equation [1, 2, 3] has been extremely successful in describing a wide range of mean-field features for experiments with Bose-Einstein condensates (BECs). In particular, the Thomas-Fermi (TF) approximation [4, 5, 6], where the kinetic energy is neglected, has been very rewarding [7]. This approximation holds for repulsive condensates with positive scattering length a and large particle numbers. In the regime of validity of the TF approximation, the total energy is distributed between interaction energy and potential energy from the confining trap, while the kinetic energy becomes negligible.

Because of the non-linear nature of the GP equation, it is only solved analytically in a few cases, e.g., vortices and solitons in homogeneous condensates [2, 3]. The TF solution is also analytical, although it only holds in the bulk of the condensate. At the surface the approximation breaks down and is usually patched by including the kinetic energy at the surface [5, 6].

The interactions of the ordinary GP equation are based on the lowest order zero-range potential, which is governed by the scattering length alone. Although this approximation is usually very good, the higher-order corrections to the scattering dynamics [8, 9, 10] can be crucial in certain cases, e.g., for Rydberg molecules embedded in BECs [10] and for narrow Feshbach resonances [11]. Inclusion of higher-order terms is well known and applied in Skyrme-Hartree-Fock calculations in nuclear physics [12]. Here, they often play a crucial role in order to get bulk nuclear properties right [13, 14]. However, the effects of similar higher-order terms in the GP equation have been less investigated.

In this paper, we solve the modified GP equation with higher-order interactions analytically in the TF approximation. The paper is organized as follows. In Sec. II, we introduce the modified GP equation and its parameters and show how it is derived from an appropriate energy density functional with careful treatment of boundary terms. We present the analytical solution in the TF ap-

proximation in Sec. III and discuss the condensate size and chemical potential as function of the interaction parameters in Sec. IV. The density profiles and energies are discussed in Sec. V, and in Sec. VI, we address the consistency of the TF approximation by considering the kinetic energy of the solutions. We compare to some relevant atomic systems in Sec. VII and finally present our conclusions in Sec. VIII.

II. MODIFIED GP EQUATION

We assume that the condensate can be described by the GP equation. Since we are interested in the ultracold regime, where the temperature is much smaller than the critical temperature for condensation, we adopt the $T = 0$ formalism. In order to include higher-order effects in the two-body scattering dynamics, we use the modified GP equation derived in [10], which in the stationary form reads

$$\mu\Psi = \left[-\frac{\hbar^2}{2m}\nabla^2 + V(r) + U_0 (|\Psi|^2 + g_2\nabla^2|\Psi|^2) \right] \Psi, \quad (1)$$

where m is the atomic mass, V is the external trap, $U_0 = 4\pi\hbar^2 a/m$, and $g_2 = a^2/3 - ar_e/2$, with a and r_e being, respectively, the s -wave scattering length and effective range [10]. We assume an isotropic trap, $V(r) = m\omega^2 r^2/2$, and introduce the trap length $b = \sqrt{\hbar/m\omega}$. The single-particle density, $\rho(r) = |\Psi(r)|^2$, is normalized to the particle number, $N = \int d\mathbf{r}\rho(r)$, and μ is the chemical potential.

As the boundary conditions are important for the TF approximation applied below we now discuss the procedure for obtaining the modified GP equation from the corresponding energy functional which is

$$E(\Psi) = \int d\mathbf{r}(\epsilon_K + \epsilon_V + \epsilon_I + \epsilon_{I2}), \quad (2)$$

with kinetic, potential, and interaction energy densities

$$\epsilon_K = \frac{\hbar^2}{2m} |\nabla\Psi|^2, \quad \epsilon_V = V(\mathbf{r})|\Psi|^2, \quad (3)$$

$$\epsilon_I = \frac{1}{2}U_0|\Psi|^4, \quad \epsilon_{I2} = \frac{1}{2}U_0g_2|\Psi|^2\nabla^2|\Psi|^2. \quad (4)$$

The corresponding integrated energy contributions are denoted E_K , E_V , E_I , and E_{I2} , respectively. To obtain Eq. (1), we vary Eq. (2) with respect to Ψ^* for fixed Ψ . To first order in $\delta\Psi^*$, we have

$$\begin{aligned} \delta E &= E[\Psi^* + \delta\Psi^*] - E[\Psi^*] \\ &= \int d\mathbf{r} \left[-\frac{\hbar^2}{2m} \nabla^2\Psi + V(\mathbf{r})\Psi \right. \\ &\quad \left. + U_0 (|\Psi|^2 + g_2\nabla^2|\Psi|^2) \Psi \right] \delta\Psi^* \\ &+ \int d\mathbf{S} \cdot |\Psi|^2 \nabla (\Psi \delta\Psi^*) - \int d\mathbf{S} \cdot \Psi \delta\Psi^* \nabla |\Psi|^2 \\ &+ \int d\mathbf{S} \cdot \delta\Psi^* \nabla \Psi. \end{aligned} \quad (5)$$

Here, \mathbf{S} is the outward-pointing surface normal. In the usual analysis, one assumes that Ψ and $\nabla\Psi$ vanishes at infinity, drops the boundary terms, and Eq. (1) is obtained by varying $E - \mu N$. However, the existence of these surface terms is essential for the inclusion of higher-order interactions as discussed below.

In the rest of this paper we use trap units, $\hbar\omega = b = 1$, i.e., energies (E , V , μ , etc.) are measured in units of $\hbar\omega$ and lengths (a , r_e , r , etc.) in units of b . Note that g_2 has dimension of length squared.

III. THOMAS-FERMI APPROXIMATION

Let us briefly review the standard Thomas-Fermi approximation [1, 2, 3, 4]. Neglecting the kinetic-energy term, as compared to the trap and interaction energies, the GP equation has the solution

$$\rho_{TF} = \frac{1}{4\pi a} (\mu_{TF} - \frac{1}{2}r^2), \quad (6)$$

with chemical potential μ_{TF} . This solution is used out to the surface, R_{TF} , while outside $\rho_{TF} = 0$. The normalization and surface condition $\rho_{TF}(R_{TF}) = 0$ give

$$\mu_{TF} = \frac{1}{2}R_{TF}^2. \quad R_{TF} = (15Na)^{1/5}. \quad (7)$$

The total energy becomes

$$\frac{E_{TF}}{N} = \frac{5}{7} \frac{R_{TF}^2}{2}. \quad (8)$$

The trap and interaction energies are $E_V = 3E/5$ and $E_I = 2E/5$, respectively. Since $R_{TF} > 0$ in Eq. (7), these results only hold for $a > 0$. The TF approximation is good for $Na \gg 1$, except at the surface region where the kinetic-energy density diverges. Here, the solution can be corrected as in [2, 3, 5, 6], essentially giving a small exponential tail.

Inclusion of higher-order interactions

We now consider the TF approximation with the higher-order interaction term, ϵ_{I2} . Ignoring the boundary terms in Eq. (5), the modified GP equation can then be written in terms of the density $\rho(r) = |\Psi(r)|^2$ as

$$\mu = \frac{1}{2}r^2 + 4\pi a (\rho + g_2\nabla^2\rho). \quad (9)$$

With scaled coordinate $x = r/\sqrt{g_2}$ (assuming $g_2 > 0$ for the moment) and density $f(r) = 4\pi a x \rho(r)/g_2$, this becomes

$$\frac{d^2f}{dx^2} + f = \frac{\mu}{g_2}x - \frac{1}{2}x^3, \quad (10)$$

The inhomogeneous and homogeneous solutions with boundary condition $f(0) = 0$ are

$$f_i(x) = \left(\frac{\mu}{g_2} - \frac{1}{2}x^2 + 3\right)x, \quad f_h(x) = \frac{A}{g_2} \sin x, \quad (11)$$

where A is a constant (with dimensions of length squared) to be determined later. The full solution is

$$\rho(x) = \frac{g_2}{4\pi a} \left[\frac{\mu}{g_2} - \frac{1}{2}x^2 + 3 + \frac{A \sin x}{g_2 x} \right]. \quad (12)$$

For a given A , the chemical potential μ and the condensate radius R are determined by the normalization and the surface condition,

$$\int_0^{x_0} 4\pi x^2 \rho(x) dx = N \quad \text{and} \quad \rho(x_0) = 0, \quad (13)$$

where $x_0 = R/\sqrt{g_2}$. The solution ρ should be positive for $x < x_0$ which must be explicitly checked. Outside x_0 , we use $\rho = 0$.

We now consider the boundary terms in Eq. (5). Above, we assumed that $\rho(x_0) = 0$ at some finite radius x_0 which we identify as the condensate size. However, only the first two boundary terms in Eq. (5) vanish on account of this condition. For the last term in Eq. (5) to vanish we need $\nabla_x \Psi(x_0) = 0$, which implies that

$$\frac{d\rho}{dx}(x_0) = 0. \quad (14)$$

Notice that this latter derivative is in fact non-zero in the $g_2 = 0$ case, which is the root of the divergence of the kinetic energy at the condensate surface as we discuss later. Equation (14) gives a closed expression for the remaining free parameter A ,

$$\frac{A}{g_2} = \frac{x_0^3}{x_0 \cos x_0 - \sin x_0}. \quad (15)$$

This additional requirement on the derivative at the edge of the condensate implies that higher-order terms require a smoothing at the surface of the cloud. In addition, the discussion of which kinetic operator structure

to use ($|\nabla\Psi|^2$ or $\Psi^*\nabla^2\Psi$ [6]) is obsolete in our treatment since the boundary term $\delta\Psi^*\nabla\Psi$ vanishes. In this sense the inclusion of a higher-order term neatly removes some of the difficulties of the traditional TF treatment.

The solutions with a finite boundary R of the modified GP equation only minimize the energy functional if Eq. (14) holds. We note that extremal states of the energy functional always satisfy the virial theorem. Thus, enforcing the virial theorem on the GP solutions is equivalent to Eq. (14). We show in the Appendix that the virial theorem approach also leads to Eq. (15).

IV. SIZE AND CHEMICAL POTENTIAL

We now determine the condensate size R and chemical potential μ . The normalization condition is

$$\frac{Na}{g_2^{5/2}} = x_0^3 \left(\frac{\mu}{3g_2} - \frac{x_0^2}{10} \right), \quad (16)$$

while the surface condition reads

$$\frac{\mu}{g_2} - x_0^2/2 + 3 + \frac{A}{g_2} \frac{\sin x_0}{x_0} = 0. \quad (17)$$

Combining eq. (15)-(17) gives

$$\frac{Na}{g_2^{5/2}} = x_0^3 \left(\frac{x_0^2}{15} - 1 + \frac{x_0^2/3}{1 - x_0 \cot x_0} \right), \quad (18)$$

which determines R for given Na and g_2 , and upon back-substitution also μ .

The $g_2 < 0$ case can be worked out analogously by replacing trigonometric functions with hyperbolics and keeping track of signs. The two cases can in fact be combined into one equation

$$\frac{Na}{|g_2|^{5/2}} = |x_0|x_0^2 \left(\frac{x_0^2}{15} - 1 + \frac{x_0^2/3}{1 - |x_0 \cot x_0|} \right). \quad (19)$$

This equation determines $x_0^2 = R^2/g_2$ implicitly as function of $Na/|g_2|^{5/2}$. The result is shown in Fig. 1. We notice that in principle, R becomes a multi-valued function. However, all the higher solutions for $g_2 > 0$ [dotted in Fig. 1] are spurious, since the density becomes negative on one or more intervals inside R . The non-spurious solutions [solid line in Fig. 1] define R as a single-valued function of a and g_2 , which was not guaranteed a priori. The four quadrants in Fig. 1 correspond to the different sign combinations of a and g_2 . The sign of the extra interaction energy, E_{I2} , is determined by $ag_2\nabla^2\rho$. For a typical concave density, the Laplacian term will be negative. We therefore see that for $ag_2 > 0$, the higher-order interaction is attractive, whereas for $ag_2 < 0$, it is repulsive. The TF solution only exists for $ag_2 < 0$. We discuss both cases separately below.

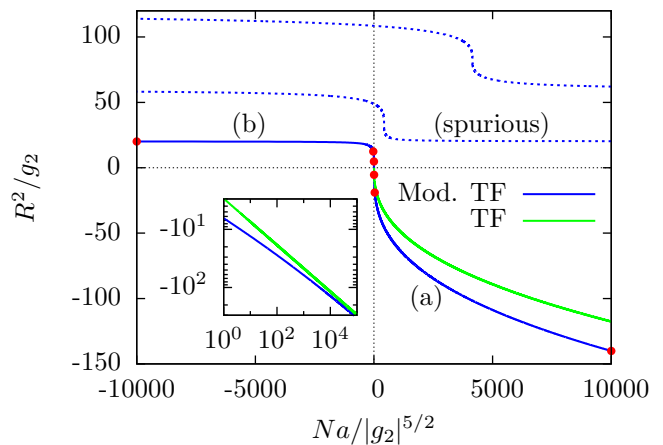


FIG. 1: (Color online) Condensate size (R) as function of Na and g_2 as found in the modified TF approximation, Eq. (19). The solutions (a) and (b) correspond to the sign combinations ($a > 0, g_2 < 0$) and ($a < 0, g_2 > 0$), respectively. No solutions exist for $ag_2 > 0$. The spurious solutions (dotted) have negative densities for one or more intervals inside R . The branch (a) approaches the normal TF result Eq. (7) when $Na \rightarrow +\infty$ or $g_2 \rightarrow -0$. Note that the convergence is only relative [see eq. (19)] and the TF limit is better represented in the logarithmic inset. Points indicate the data from Tab. I. All values are in trap units.

A. The attractive regime: $ag_2 > 0$

For $a < 0, g_2 < 0$ [third quadrant in Fig. 1] there are no solutions, which is expected since the normal TF approximation has no solutions for $a < 0$ as the interaction energy E_I is negative and the kinetic energy that could prevent collapse is neglected.

The $g_2 > 0, a > 0$ case in the first quadrant has only spurious solutions. Here the g_2 term is attractive for the typical concave density and a collapse towards a high-density state is possible in complete analogy to the usual discussion of attractively interacting condensates within the standard GP theory. Whereas there can be metastable states at large values of $Na/g_2^{5/2}$, these are stabilized by kinetic energy and thus are not present in our TF approach. Thus, even when the total kinetic energy is small, it is still needed to prevent the attractive higher-order term from amplifying local-density variations.

This important point can also be established by considering the stability of the homogeneous condensate through linearization of the GP equation. By repeating the analysis of [2] with the higher-order term, we find that for $g_2 > 0$ and $a > 0$, the kinetic-energy term is crucial for the stability of the excitation modes. In fact, exponentially growing modes will always be present if the kinetic energy is neglected. This will be discussed elsewhere in relation to the numerical solution of the full GP equation [15].

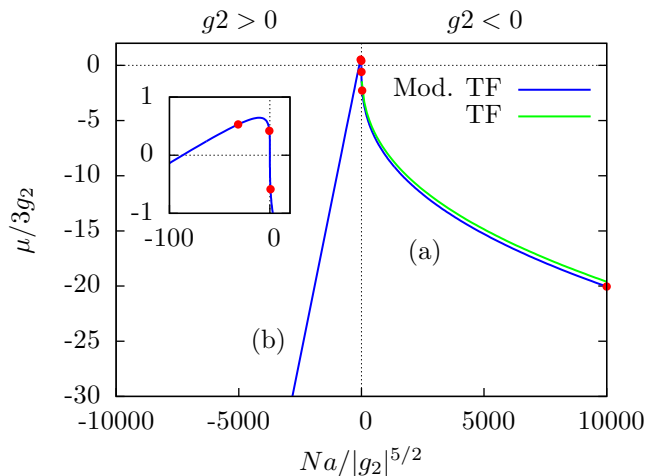


FIG. 2: (Color online) Chemical potential μ as function of Na and g_2 as found in the modified TF approximation, using the solutions (a) and (b) from Fig. 1. For branch (a) and the upper part of branch (b) (see inset), we have $\mu > 0$. The lower part of (b) has $\mu < 0$. Points indicate data from Tab. I. All values are in trap units.

B. The repulsive regime: $ag_2 < 0$

For $g_2 < 0$, $a > 0$ a single solution (a) exists. This was expected since $E_{I2} > 0$ gives extra stability. The solution approaches the normal TF result in Eq. (7) when $Na/|g_2|^{5/2} \rightarrow +\infty$, as can also be seen from Eq. (19). Of course in this limit $E_{I2} \ll E_I$. However, the -1 term in Eq. (19) implies that the convergence to the normal TF solution is only on a relative scale and is better represented on a logarithmic scale as in the inset in Fig. 1.

For $g_2 > 0$, $a < 0$ there is a single solution (b) which connects smoothly to the (a) solution. In the limit $Na/|g_2|^{5/2} \rightarrow -\infty$, which is determined by $x_0 \cot x_0 = 1$, we find $R^2/g_2 = 20.1907$. This solution is possible when the g_2 term provides just enough repulsion to cancel the usual $a < 0$ collapse behavior.

C. Chemical potential

In Fig. 2 we show the chemical potential for the smoothly connecting solutions (a) and (b). Again we see that (a) approaches the normal TF limit for large $Na/|g_2|^{5/2}$. Here, it is interesting to note how μ turns around near the origin [amplified in the inset in Fig. 2] and maintains a positive value. This occurs in the region where the lowest-order interaction gives a large negative-energy contribution which the g_2 term is still able to balance yielding a well-defined TF solution. This behavior is analogous to the balancing of attraction by the kinetic term in the usual $a < 0, g_2 = 0$ case [1, 4]. As a becomes increasingly negative, so too does μ and collapse is inevitable (and likewise when $g_2 \rightarrow 0^+$).

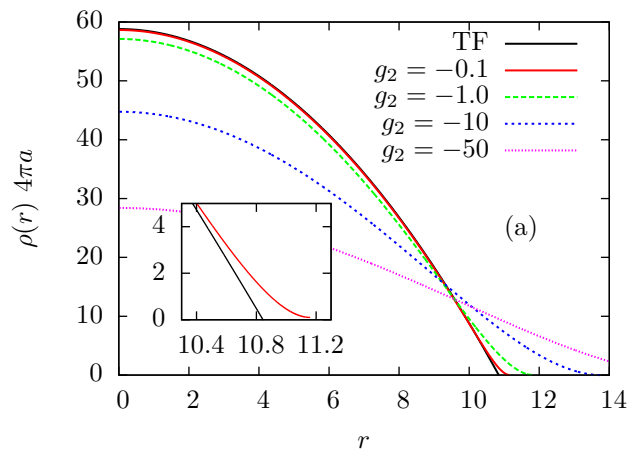


FIG. 3: (Color online) Densities for branch (a) in Fig. 1 ($g_2 < 0$ and $Na = 10^4$). The $g_2 = -0.1$ curve is on top of the normal TF result. Inset shows the smooth behavior at the surface for $g_2 < 0$. All values are in trap units.

V. DENSITIES AND ENERGIES

With R and μ determined, we can find the density profile, energy densities and integrated energy contributions. With Eq. (12), the energy densities are given by

$$\epsilon_V = \frac{x^2}{2}\rho, \quad \epsilon_I = 2\pi a\rho^2, \quad (20)$$

$$\epsilon_{I2} = -\frac{1}{2}\rho\left(3 + \frac{A}{g_2} \frac{\sin x}{x}\right). \quad (21)$$

Using Eq. (9), the total energy density (without ϵ_K) becomes

$$\epsilon \equiv \epsilon_V + \epsilon_I + \epsilon_{I2} = \frac{1}{2}\rho(x)(V(x) + \frac{\mu}{g_2}). \quad (22)$$

In Fig. 3, we show the density profile of the (a) solutions for $Na = 10^4$ and selected $g_2 < 0$. We clearly see that the higher-order term tends to expand the condensate through its repulsion. Importantly, at the boundary, there is a smoothing caused by the condition in Eq. (14) [see inset in Fig. 3]. We will discuss how this affects the estimated kinetic energy in the next section. As $|g_2|$ grows, we see the condensate flatten and in the limit of very large $|g_2|$, it becomes a constant density.

Figure 4 displays the density profile for the (b) solutions with $a < 0$ for selected $g_2 > 0$. Here, we see the profile collapse toward the expected delta-function with decreasing g_2 . It is interesting to follow the (a) solution through the origin in Fig. 1 and onto solution branch (b), passing from $g_2 = -\infty$ to $g_2 = \infty$. On the (a) branch, the solution flattens as g_2 decreases and eventually becomes effectively constant in space. This is also true for the (b) branch at $g_2 = \infty$, and as g_2 is decreased, the solution proceeds to shrink as the g_2 term becomes unable to provide the repulsion needed to prevent the $a < 0$ collapse induced by the lowest-order term.

From the figures, we see that large $|g_2|$ induces large changes in cloud size. As the condensate can be imaged

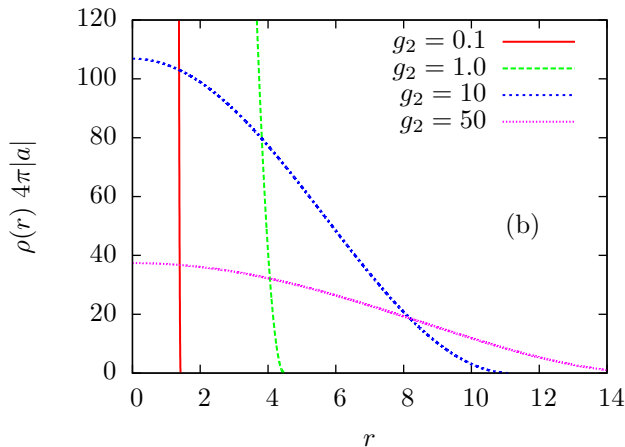


FIG. 4: (Color online) Same as Fig. 1 but for solutions (b), i.e., opposite signs $g_2 < 0$ and $Na = -10^4$.

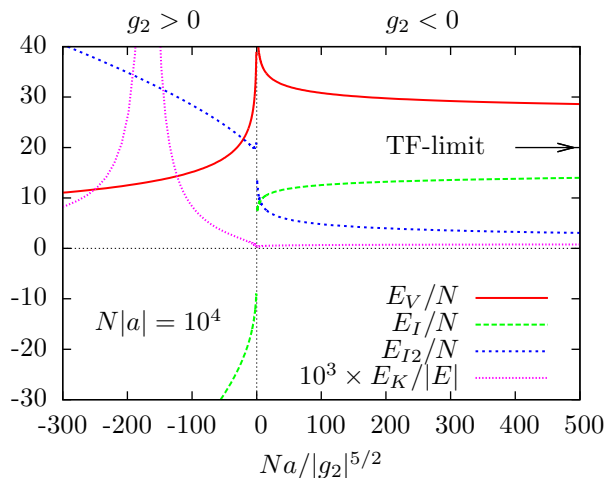


FIG. 5: (Color online) Different total-energy contributions. $N|a| = 10^4$. All values are in trap units.

with very good resolution [7], this should be measurable if the regime of large $|g_2|$ can be accessed.

We now discuss the energy contributions which are interesting since the release energies are in fact measurable quantities [3]. Since we neglect the kinetic term in the TF approximation, the release energy is simply $E_R = E_I + E_{I2} = E - E_V$. In Tab. I, we give the integrated energy contributions for some relevant values of g_2 calculated for $N|a| = 10^4$, whereas Fig. 5 gives the energies as function of $Na/|g_2|^{5/2}$. We note that for smaller values of $N|a|$, the same overall behavior is found, however, the kinetic term is more important and the TF approximation becomes worse.

We observe that E/N grows towards the $|g_2| = \infty$ point. This is due to the trap energy increasing as the density flattens [E_V diverges around the origin in Fig. 5]. Furthermore, as $g_2 \rightarrow 0^+$ the energy diverges toward $-\infty$ as the collapse sets in [E_I diverges on the $g_2 > 0$ side in Fig. 5]. The boundary where the energy vanishes is

around $g_2 = 5.14$ for $N|a| = 10^4$, but this depends on the choice of $N|a|$. With respect to the release energy, we find that somewhere in the region $10 < g_2 < 50$, E_R becomes negative. This is a result of the unavoidable collapse, and also indicates that kinetic energy cannot be ignored at this point. Notice, however, that the release energy changes considerably and could provide a way to measure the influence of the g_2 term.

VI. CONSISTENCY OF THE THOMAS-FERMI APPROXIMATION

We now address the validity of the TF approximation with the g_2 term included. In order to do so, we must consider the contribution of the kinetic energy. The kinetic energy density can be written as

$$\epsilon_K = \frac{g_2}{8\rho(4\pi a)^2} \left(x + \frac{A}{g_2} \frac{x \sin x - \cos x}{x} \right)^2. \quad (23)$$

Strictly speaking, this is not the true kinetic energy, since the kinetic terms were neglected from the start. However Eqs. (22) and (23) can be used to test whether the TF approximation holds locally, i.e., $\epsilon_K \ll \epsilon$ should hold for the solution ρ to be consistent. In Tab. I, we calculate the integrated contribution of the kinetic energy relative to the total TF energy and we find that the contribution is small everywhere except the point where $E = 0$ on the $g_2 > 0$ side of Fig. 5. Here, the kinetic energy is of course the most important term and the TF approximation is poor.

In the standard TF, the kinetic energy causes trouble at the boundary of the cloud. Here, $\nabla\Psi \propto \nabla\rho/\sqrt{\rho}$ and since the density vanishes and the derivative is finite [see Eq. 6], this diverges at R_{TF} . When including the higher-order term we need to use the additional boundary condition $\nabla\Psi = 0$ at R , so the kinetic energy will be strictly zero at R . However, as one approaches the boundary, the kinetic-energy density grows rapidly before it descends towards zero within a very small interval at R . The total energy density in Eq. (22) goes to zero at this point and we find that ϵ_K/ϵ is very large near the boundary as in the usual $g_2 = 0$ case.

We conclude that the inclusion of the higher-order term does not alleviate the difficulties with kinetic energy at the boundary. The techniques for addressing this problem described in [5, 6] should therefore be generalized to include the higher-order interaction term in order to improve the description at the boundary of the cloud.

VII. COMPARISON TO ATOMIC SYSTEMS

The considerations above show that deviations from the usual TF approximation can be strong when g_2 is large. In the following, we reintroduce explicit units for comparison with real systems. We have to consider g_2/b^2 .

	g_2	R	μ	E_V/N	E_I/N	E_{I_2}/N	E/N	E_R/N	$E_K/ E $
TF	—	10.8447	58.8040	25.2017	16.8011	—	42.0028	16.8012	3.135×10^{-3} ^a
(a)	-0.01	10.9447	58.8188	25.2164	16.7865	0.01465	42.0176	16.8012	1.8×10^{-3}
	-0.1	11.1607	58.9481	25.3430	16.6635	0.13909	42.1456	16.8026	1.4×10^{-3}
	-1.0 ^b	11.8364	60.1210	26.4309	15.6818	1.16330	43.2760	16.8451	1.0×10^{-3}
	-10 ^b	13.7835	68.4515	32.9856	11.3469	6.38609	50.7186	17.7330	0.57×10^{-3}
	-50 ^b	16.439	87.8248	45.6836	6.99293	14.0777	66.7542	21.0706	0.30×10^{-3}
(b)	50 ^b	15.407	63.0102	38.9723	-8.92496	20.9439	50.9912	12.0189	0.43×10^{-3}
	10 ^b	11.170	15.9128	19.8375	-24.7434	22.7810	17.8751	-1.9623	2.3×10^{-3}
	5.14 ^c	9.1999	-13.1384	13.1579	-46.0283	32.8801	0.0097	-13.148	6.098
	1.0 ^b	4.4801	-327.612	3.04199	-416.359	251.032	-162.285	-165.33	1.5×10^{-3}
	0.1	1.4204	-10456.4	0.30571	-13071.1	7842.81	-5227.98	-5228.4	0.47×10^{-3}

^aThe kinetic energy estimated by surface corrections as in [2].

^bValues are indicated by points in Figs. 1 and 2.

^cThe total energy $|E|$ is zero near $g_2 = 5.14$, hence the TF approximation is invalid here.

TABLE I: Chemical potential μ and condensate size R for different g_2 and fixed $N|a| = 10^4$. The integrated energies are trap (E_V), interaction (E_I, E_{I_2}), total ($E = E_V + E_I + E_{I_2}$), and release energy ($E_R = E - E_V$). The TF limit is approached for $g_2 \rightarrow -0$. The ratio of kinetic energy E_K to total energy E indicates where the TF approximation is valid. The corresponding density distributions are shown in Figs. 3 and 4. All values are in trap units.

Of course, the b^2 factor means that this quantity is generally very small since g_2 is of order a_0^2 and b is of order $10^4 a_0$.

We first consider some typical background values for bosonic alkali atoms away from resonance. We estimate the effective range to be the of order of the potential range and assuming a van der Waals interaction, we have $r_e \sim 50 - 200 a_0$. For typical one-component gases we have $-450 a_0 \lesssim a \lesssim 2500 a_0$ [16]. Since $g_2 = a^2/3 - ar_e/2$, we see that the a^2 term will dominate and in all cases $0 < g_2 \lesssim 10^6 a_0$. In trap units, this becomes $g_2/b^2 \lesssim 5 \cdot 10^{-3} (1 \mu\text{m}/b)^2$. In typical traps of $b \sim 1 - 10 \mu\text{m}$, the higher-order term is therefore very small. These values also predominantly lie in the first quadrant of Fig. 1 and thus no TF solution exists.

Let us first consider Feshbach resonances in order to increase the influence of the g_2 term. We use a multi-channel Feshbach model [17], which describes the full T matrix as a function of resonance position B_0 , width ΔB , magnetic-moment difference between the channels $\Delta\mu$, and the background scattering length a_{bg} . Performing an effective-range expansion [11], we have $a = a_{bg}[1 - \Delta B/(B - B_0)]$ and $r_e = r_{e0}/[1 - (B - B_0)/\Delta B]^2$, where $r_{e0} = -2\hbar^2/ma_{bg}\Delta\mu\Delta B < 0$. Combining these relations, we find $r_e = r_{e0}(1 - a_{bg}/a)^2$ and

$$g_2(a) = \frac{a^2}{3} - \frac{ar_{e0}}{2} \left(1 - \frac{a_{bg}}{a}\right)^2. \quad (24)$$

Hence g_2 diverges when $a \rightarrow 0$ (referred to as zero-crossing) or $a \rightarrow \infty$ (on resonance). Near zero crossing, the effective-range expansion is, however, severely divergent and its validity is questionable. Even so, the effective-range corrections near zero-crossing obtained are in fact identical to those obtained from use of the full T-matrix [18]. One finds $\lim_{a \rightarrow 0} ag_2 = |r_{e0}|a_{bg}^2/2$, where $r_{e0} < 0$.

As a concrete example, we consider the alkali isotope ^{39}K where several Feshbach resonances of vastly different widths were found recently [19]. First, we focus on zero-crossing and consider the very narrow resonance at $B_0 = 28.85\text{G}$ with $\Delta B = -0.47\text{G}$, $\Delta\mu = 1.5\mu_B$, and $a_{bg} = -33a_0$. We obtain $r_{e0} = -5687a_0$ and $ag_2 \rightarrow 93.8 \cdot 10^3 a_0^3$ for $a \rightarrow 0$. It is important to notice that $ag_2 > 0$ around $a = 0$. This means that we are looking for solutions in the first and third quadrants of Fig. 1 and again we have to conclude that no TF solutions can be found when higher-order terms are taken into account.

Another case of interest is around resonance where $|a| = \infty$. Here, we have $r_e \sim r_{e0}$ and $g_2 \propto a^2 > 0$ on both sides of the resonance. Thus, the $a > 0$ side will be in the first and the $a < 0$ in the second quadrant of Fig. 1. This makes it difficult to imagine sweeping the resonance from either side to probe the solutions on branch (b) in Fig. 1. One could imagine starting on the $a > 0$ side with small $g_2 > 0$. The full GP equation will have perfectly sensible solution here, however, when one approaches the resonance the g_2 term will diverge and induce collapse already on the $a > 0$ side. If we approach from the $a < 0$ side, then we face the problem that the critical number of particles decreases dramatically before g_2 grows sufficiently and one therefore needs a very small condensate since $Na/b \sim 0.5$ [11]. At this point, the TF approximation is no longer valid.

The Feshbach resonance used to increase g_2 must be very narrow in order for r_{e0} to be large. However, most experimentally known resonances are not narrow. For broad or intermediate resonances, we have to consider the long-range van der Waals interaction when calculating the effective-range corrections. Analytic formulas for this case have been worked out in [20], and we note that the effective range diverges as a^{-2} near zero crossing exactly as in the Feshbach model above. For very narrow

resonances, we still have $\beta_6 \ll r_{e0}$, where β_6 is the characteristic length of the van der Waals interaction. The model above should thus give the dominant contribution.

Using the van der Waals formulas we can estimate ag_2 at zero crossing. We find

$$\frac{ag_2}{b^3} \rightarrow -\frac{1}{3x_e} \left(\frac{\beta_6}{b} \right)^3, \quad (25)$$

where $x_e = (\Gamma[1/4])^2/2\pi$, with Γ the gamma function. We have explicitly introduced the oscillator length which is the relevant length scale of comparison. Importantly, we find that $ag_2 < 0$ for $a > 0$ and we are thus in the fourth quadrant where a TF solution exists. For $a < 0$, we pass to the second quadrant as g_2 becomes positive and a single collapsed solution can be found.

We now estimate the parameters obtained from the van der Waals formulas. With $b = 1\mu\text{m}$ and $\beta_6 \sim 123.3a_0$ [2], we have $ag_2/b^3 \sim -10^{-8}$. We thus have $Na/|g_2|^{5/2} \propto 10^8(Na)a^{5/2}$. For values of a that are not extremely small, the solution is therefore typically located far to the right in Fig. 1 where it will look similar to the $g_2 = 0$ case. We can estimate how close to zero one would have to tune a in order to see deviations using the $a \rightarrow 0$ limit of the van der Waals effective range. Let us aim for $g_2/b^2 = -10$ which should be observable in the condensate profile according to Fig. 3. With $b = 1\mu\text{m}$, we need $a \sim 10^{-6}\beta_6 \sim 1.7 \times 10^{-4}a_0$. Using broad resonances, one can tune to zero at the level of $10^{-2}a_0$ in ^{39}K [21]. Observing the effect of the g_2 term therefore seems out of reach at the moment, but might be possible in the near future. Of course, we still have to maintain a large value of Na for kinetic energy to be small, and thus a larger condensate is needed close to zero crossing.

From the examples above, we see problems in accessing the TF solutions presented above in current experiments with ultracold alkali gases. In particular, we notice that realistic systems which have been used for creation of BECs in alkali-metal gases for the last decades have parameters that predominantly lie in the first quadrant of Fig. 1. As we have discussed, there are no well-defined TF solutions in that region. Therefore, we see that the kinetic energy plays a decisive role and we are forced to consider it in principle, even if it is small for all practical purposes. The physical reason is that for $a > 0$ and $g_2 > 0$, the higher-order interaction is effectively attractive and induces collapse which will have to be balanced by a barrier from the kinetic term, similar to the $a < 0$, $g_2 = 0$ case [1]. Since we neglect the kinetic term in the TF approximation, we should not expect to find solutions in the $ag_2 > 0$ case.

Only in the case of resonances dominated by the long-range van der Waals interaction do the parameters allow for TF solutions with non-zero g_2 . However, here the length scale of the trap makes the contribution very small and the TF solution becomes identical to the $g_2 = 0$ case. One could in principle tune a very close to zero-crossing and obtain a significant contribution but the level of tuning required is beyond current experimental reach.

VIII. CONCLUSIONS

We have considered the effect of higher-order interactions in Bose-Einstein condensates within the Gross-Pitaevskii theory. We derived the GP equation with effective-range corrections included and solved it analytically in the Thomas-Fermi approximation. Higher-order interaction terms act as derivatives on the condensate wave function which means that the boundary conditions on the solutions of the GP equation must be carefully considered. We then discussed the solutions for various parameters and presented the chemical potential, density profiles, and the energy contributions.

We find that no TF solutions are possible when the higher-order term is attractive. This conclusion holds both in the trapped system and in the homogeneous case [15]. An estimate of the relevant parameters for alkali atoms showed that away from resonances, they typically lie in the region where the effective-range correction is effectively attractive and likewise near very narrow Feshbach resonances. We conclude that in those cases, the kinetic energy, even if very small, is crucial in order to stabilize collapse due to higher-order interaction terms. For broader resonances where the long-range van der Waals potential is dominant, we find that modified TF solutions exist. However, for typical traps, the parameters are very small and tuning of the scattering length near zero crossing at a level beyond current experimental reach is necessary. This might of course become possible as experimental control improves in the future.

ACKNOWLEDGMENTS Discussions with D. V. Fedorov, N. Nygaard, and I. Zapata are highly appreciated.

APPENDIX A: DETERMINATION OF A FROM THE VIRIAL EQUATION

Even though Eq. (12) is a solution to the modified GP equation Eq. (9) for all A , it does not necessarily minimize the energy functional as discussed in the main text. This can also be seen from the virial equation (with neglected kinetic energy),

$$-2E_V + 3E_I + 5E_{I2} = 0, \quad (\text{A1})$$

which holds for all extremal points of the energy functional. Equation (A1) is derived from the energy functional using scaling arguments as in [3].

As an example, consider the $A = 0$ solution in Eq. (12). This solution has a chemical potential shifted by $3g_2$ compared to the $g_2 = 0$ TF result. But the density is unchanged and so is E_V and E_I . Hence, the usual virial equation $-2E_V + 3E_I = 0$ for $g_2 = 0$ also holds for $g_2 \neq 0$. Since $E_{I2} = -3g_2/2 \neq 0$, the virial equation Eq. (A1) is not fulfilled, and hence the $A = 0$ solution is not extremal. Below, we use the virial equation to calculate the value of A that minimizes the energy functional and the corresponding R and μ . We will also

prove that this condition is in fact equivalent to assume $\rho(x_0) = \nabla_x \rho(x_0) = 0$ at the boundary.

The general results for A , R , and μ can be derived using the normalization and surface conditions Eq. (13), and the virial equation Eq. (A1). For convenience, we introduce the variables $\bar{\mu} = \mu/(3g_2) + 1$, $\bar{A} = A/(3g_2)$, and $c = Na/g_2^{5/2}$. The different energy contributions are

$$\begin{aligned} E_V &= 3s \int_0^{x_0} dx x^4 \left(\bar{\mu} - \frac{x^2}{6} + \bar{A} \frac{\sin x}{x} \right), \\ E_I &= 9s \int_0^{x_0} dx x^2 \left(\bar{\mu} - \frac{x^2}{6} + \bar{A} \frac{\sin x}{x} \right)^2, \\ E_{I2} &= -9s \int_0^{x_0} dx x^2 \left(\bar{\mu} - \frac{x^2}{6} + \bar{A} \frac{\sin x}{x} \right) \left(1 + \bar{A} \frac{\sin x}{x} \right), \end{aligned} \quad (\text{A2})$$

where $s = g_2^{7/2}/(2a)$. Direct integration of Eq. (A2),

insertion of $\bar{\mu}$ from Eq. (17), and some algebra gives the virial equation

$$\begin{aligned} 0 &= -2E_V + 3E_I + 5E_{I2} \\ &= -\frac{s}{x_0} (x_0^3 - 3\bar{A}(x_0 \cos x_0 - \sin x_0))^2. \end{aligned} \quad (\text{A3})$$

We immediately see that this is in fact equivalent to Eq. (15). Therefore, the solution we have explicitly found above minimizes the energy functional with boundary conditions $\rho(x_0) = \nabla_x \rho(x_0) = 0$. More generally, when we solved the modified GP equation without considering the boundary terms in Sec. (III), we found a one-parameter family of solutions (parametrized by A). The virial theorem is merely a constraint on A for obtaining a minimum of E .

-
- [1] F. Dalfovo, S. Giorgini, L. P. Pitaevskii, and S. Stringari, *Rev. Mod. Phys.* **71**, 463 (1999).
- [2] C. J. Pethick and H. Smith, *Bose-Einstein Condensation in Dilute Gases*, (Cambridge University Press, London, 2002).
- [3] L. P. Pitaevskii and S. Stringari, *Bose-Einstein Condensation*, The International Series of Monographs on Physics (Oxford University Press, New York, 2003).
- [4] G. Baym and C. J. Pethick, *Phys. Rev. Lett.* **76**, 6 (1996).
- [5] F. Dalfovo, L. Pitaevskii, and S. Stringari, *Phys. Rev. A* **54**, 4213 (1996).
- [6] E. Lundh, C. J. Pethick, and H. Smith, *Phys. Rev. A* **55**, 2126 (1997).
- [7] L. Vestergaard Hau, B. D. Busch, C. Liu, Z. Dutton, M. M. Burns, and J. A. Golovchenko, *Phys. Rev. A* **58**, R54 (1998).
- [8] R. Roth and H. Feldmeier, *Phys. Rev. A* **64**, 043603 (2001).
- [9] H. Fu, Y. Wang and B. Gao, *Phys. Rev. A* **67**, 053612 (2003).
- [10] A. Collin, P. Massignan, and C. J. Pethick, *Phys. Rev. A* **75**, 013615 (2007).
- [11] N. T. Zinner and M. Thøgersen, *Phys. Rev. A* **80**, 023607 (2009).
- [12] M. Brack, C. Guet, and H.-B. Håkansson, *Phys. Rep.* **123**, 275 (1985).
- [13] T. H. R. Skyrme, *Philos. Mag.* **1**, 1043 (1956).
- [14] P. J. Siemens and A. S. Jensen, *Elements of Nuclei* (Addison-Wesley, Reading, MA, 1987).
- [15] M. Thøgersen and N. T. Zinner, to be submitted.
- [16] C. Chin, R. Grimm, P. Julienne, and E. Tiesinga, e-print arXiv:0812.1496.
- [17] G. M. Bruun, A. D. Jackson, and E. E. Kolomeitsev, *Phys. Rev. A* **71**, 052713 (2005).
- [18] N. T. Zinner, e-print arXiv:0909.1314.
- [19] C. D'Errico *et al.*, *New J. Phys.* **9**, 223 (2007).
- [20] B. Gao, *Phys. Rev. A* **58**, 4222 (1998).
- [21] M. Fattori, C. D'Errico, G. Roati, M. Zaccanti, M. Jonas-Lasinio, M. Modugno, M. Inguscio, and G. Modugno, *Phys. Rev. Lett.* **100**, 080405 (2008).